Available online at www.sciencedirect.com
ScienceDirect
Applied Acoustics 68 (2007) 1468–1484
applied acoustics
www.elsevier.com/locate/apacoust

Improvements to the Johnson–Allard model for rigid-framed fibrous materials

Naoki Kino *, Takayasu Ueno

Shizuoka Industrial Research Institute of Shizuoka Prefecture, 2078 Makigaya, Aoi-ku, Shizuoka, Shizuoka 421-1298, Japan

Received 21 November 2005; received in revised form 22 June 2006; accepted 10 July 2006
Available online 22 September 2006

Abstract

Measurements of the surface impedance and the physical parameters of seven glass wool samples and six polyester fibre samples with flow resistivities between 4100 and 69,900 Pa s m^{-2} have been made. Comparisons of measured absorption coefficients and those predicted from the Johnson–Allard formulae using the measured and deduced physical parameters show discrepancies that exceed 20% for some samples and frequencies. By modifying the Johnson–Allard formula for effective density and by introducing a correction factor that is a function of flow resistivity based on data fitting, it has been found possible to improve the predictions. However, it has also been found that a similar modification of the formula for bulk modulus is necessary to reduce the discrepancies with data to below 5% in the frequency range between 800 Hz and 5 kHz.

Keywords: Flow resistivity; Tortuosity; Viscous characteristic length, Thermal characteristic length

1. Introduction

Adequate models for predicting the acoustical properties of fibrous materials are important in the building acoustics. Although based on many measurements, the semi-empirical single-parameter (flow resistivity) model of Delany and Bazley [1] has been

* Corresponding author. Tel.: +81 54 278 3027; fax: +81 54 278 3066.
E-mail address: nkino@s-iri.pref.shizuoka.jp (N. Kino).

0003-682X/$ - see front matter © 2006 Elsevier Ltd. All rights reserved.
doi:10.1016/j.apacoust.2006.07.005

found to have some shortcomings [2]. A more comprehensive semi-empirical model, the Johnson–Allard model [3–7], requires five parameters introducing porosity, tortuosity and two characteristic lengths in addition to flow resistivity. In Section 2, careful measurements of the acoustical and physical properties of glass wool and polyester fibre materials are described. Using the measured and calculated parameter values, it is shown that the Johnson–Allard model does not perform noticeably better than the single-parameter Delany and Bazley model and that both give rise to substantial discrepancies between predictions and data for normal incidence absorption coefficient. Subsequently, in Section 3, the Johnson–Allard expressions for effective density and bulk modulus are re-expressed and modified empirically through two correction factors based on data fitting. In Section 4, it is shown that the new form of the Johnson–Allard model gives significant improvements in the agreement between predictions and data. Finally, Section 5 presents concluding remarks.

2. Measurements and model comparisons

2.1. Material

Table 1 details the seven glass wool samples and Table 2 the six polyester fibre samples used in the experiment.

2.2. Performance of the Johnson–Allard model

The measured four physical parameters and the calculated porosity were substituted for the Johnson–Allard model. The prediction error of the normal incidence absorption

Table 1
Measurements of the glass wool samples, except porosity, obtained by calculation

Sample	Sample 1	Sample 2	Sample 3	Sample 4	Sample 5	Sample 6	Sample 7
ρ_1 (kg m^{-3})	28.0	31.8	41.7	52.6	81.2	101.2	84.7
b (mm)	25.0	25.0	24.5	25.0	10.0	14.0	14.0
σ (Pa s m^{-2})	11,900	16,800	21,500	29,000	49,000	69,900	53,300
α_∞	1.0108	1.0093	1.0124	1.0144	1.0295	1.0358	1.0304
$\wedge$ (μm)	143	132	106	87	57	48	52
$\wedge'$ (μm)	302	237	225	184	123	97	126
ϕ	0.989	0.987	0.983	0.979	0.968	0.960	0.966

Table 2
Measurements of the polyester fibre samples, except porosity, obtained by calculation

Sample	Sample 10	Sample 11	Sample 12	Sample 13	Sample 14	Sample 15
ρ_1 (kg m^{-3})	35.9	72.9	49.8	72.8	49.9	64.4
b (mm)	14.0	12.5	10.5	10.5	12.0	11.0
σ (Pa s m^{-2})	19,700	51,000	9800	17,400	4100	5700
α_∞	1.0206	1.0471	1.0328	1.0494	1.0354	1.0464
$\wedge$ (μm)	125	67	152	113	269	206
$\wedge'$ (μm)	221	128	292	218	541	399
ϕ	0.974	0.947	0.964	0.947	0.964	0.953

coefficient of the Johnson–Allard model was examined in the frequency range between 100 Hz and 5 kHz. The prediction error rate was calculated by

$$100 \times |\alpha_m - \alpha_p|/\alpha_m, \tag{1}$$

where α_m is the measured frequency-dependent narrow band absorption coefficient and α_p is the predicted frequency-dependent narrow band absorption coefficient. The comparative results are shown in Fig. 1. The mean value of the prediction error of sample 2 shown in Fig. 1a was 6.2%; that of sample 6 shown in Fig. 1b was 7.1%; that of sample 11 shown in Fig. 1c was 10.6%; and that of sample 15 shown in Fig. 1d was 36.7%.

2.3. Performance of the Delany and Bazley model

The measured flow resistivities were substituted in the Delany and Bazley model. The prediction error of the normal incidence absorption coefficient of the Delany and Bazley model was examined in the frequency range between 100 Hz and 5 kHz. The comparative results are shown in Fig. 2. The mean value of the prediction error of sample 2 shown in Fig. 2a was 7.9%; that of sample 6 shown in Fig. 2b was 15.4%; that of sample 11 shown in Fig. 2c was 13.2% ; and that of sample 15 shown in Fig. 2d was 22.6%.

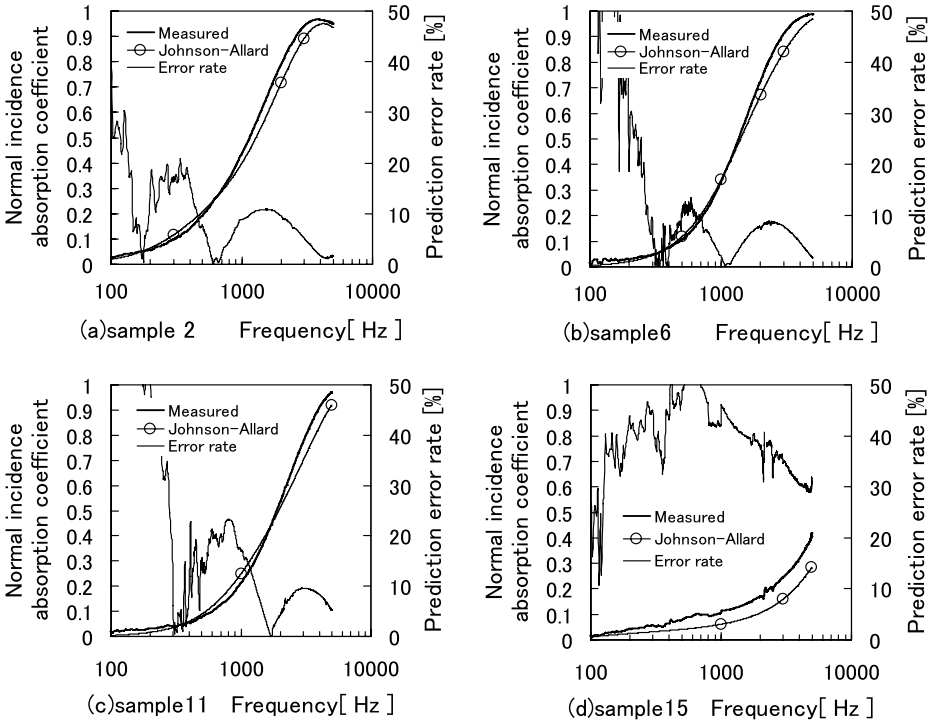

Fig. 1. Comparison of normal incidence absorption coefficients for hard-backed material samples, between the values as measured and those predicted, by the Johnson–Allard model as a function of frequency: (a) sample 2 of glass wool; (b) sample 6 of glass wool; (c) sample 11 of polyester fibre; and (d) sample 15 of polyester fibre.

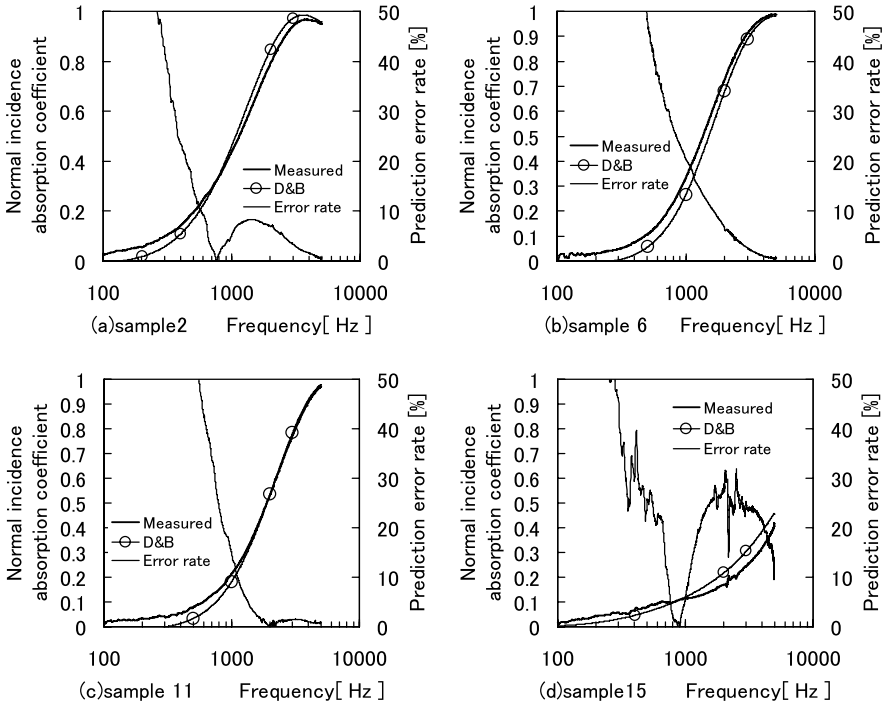

Fig. 2. Comparison of normal incidence absorption coefficients for hard-backed material samples, between the values as measured and those predicted, by the Delany and Bazley model as a function of frequency: (a) sample 2 of glass wool; (b) sample 6 of glass wool; (c) sample 11 of polyester fibre; and (d) sample 15 of polyester fibre.

2.4. Measurement of the four physical parameters

Flow resistivity was measured with a device based on the ISO standard 9053 [8]. As the predicted values in Fig. 2 tended to be close to the measurements, the values of the measured flow resistivities were judged to be sufficiently accurate.

Tortuosity and the two characteristic lengths were measured by the Sl (slope) method [9] proposed by Leclaire et al. The accuracy of these measurements was tested by using the measured values to predict the sound speed through Eq. (2) [10]. Subsequently, the predicted and measured sound speeds were compared as shown in Fig. 3. The predicted values were very close to the measured values, so that the measured values of the tortuosity and two characteristic lengths were judged to be accurate:

$$c_{\text{high}} = \frac{c_0}{\sqrt{\alpha_\infty}}\left[1 - \frac{\delta}{2}\left(\frac{1}{\wedge} + \frac{\gamma - 1}{\sqrt{Pr}\wedge'}\right)\right], \tag{2}$$

where c_{high} is the sound velocity in the materials at high frequencies, c_0 is the sound velocity in a gas, δ is the viscous skin depth, α_∞ is the tortuosity, $\wedge$ is the viscous characteristic length, $\wedge'$ is the thermal characteristic length , Pr is the Prandtl number of a gas, and γ is the specific heat ratio of a gas.

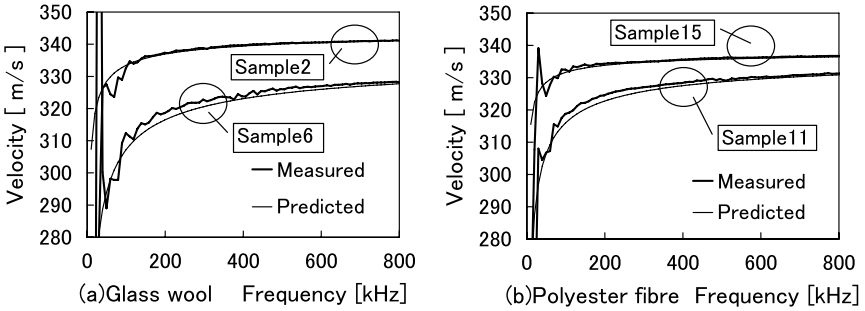

Fig. 3. Comparison between the measured and predicted sound velocities saturated by air as a function of frequency: (a) glass wool samples and (b) polyester fibre samples.

2.5. Calculation of porosity

Porosity was not measured but calculated instead using the following equation:

$$\phi = 1 - \rho_1/\rho_m, \tag{3}$$

where ϕ is the porosity, ρ_1 is the bulk density of glass wool, and ρ_m is the density of raw material of the sound absorbing materials.

The value of 2500 kg m^{-3} for the density of the glass was substituted for ρ_m to determine the glass wool samples. The value of 1380 kg m^{-3} for the density of polyethylene (PET) was similarly substituted for ρ_m to determine the porosity of the polyester fibre samples.

2.6. Measurement of normal acoustic impedance

Impedance measurements were carried out using the ISO transfer function method [11]. By reducing the inner diameters of the impedance tubes, high frequency measurement becomes possible; however, a disadvantage is that measurement accuracy at low frequencies is sacrificed. Additionally, as it is difficult to cut materials of a small diameter, an impedance tube with internal diameter of 40 mm was utilized. The lack of measurement accuracy in the low frequency range was apparent in the results of measurements of the imaginary part of the characteristic impedance at 300 Hz or less. The material characteristics in a sheet can differ according to the part of the sheet, meaning that the characteristics of two pieces of materials cut from the same sheet can differ. The use of two tubes with inner diameters of 100 mm and 29 mm introduces the undesirable problem of measurement discontinuity.

2.7. Examination of the prediction error in the Johnson–Allard model

Figs. 1 and 2 show that the performance of the Johnson–Allard model is better than that of the Delany and Bazley model at frequencies less than 1 kHz. However, the prediction error in the Johnson–Allard model was larger than that of the Delany and Bazley model at high frequencies, so the propagation constant and characteristic impedance were examined.

The propagation constant and characteristic impedance were calculated from two measurements of the surface impedance of a layer of material with different thickness of rear air layer [12]. The characteristic impedance Z_c was calculated by Eq. (4), while the propagation constant γ was calculated by Eq. (5). When the thickness of the rear air layer was set to L_0, the normal acoustic impedance Z_1 on the surface of the material was measured. As well, when the thickness of the rear air layer was changed to L_1, the normal acoustic impedance Z_1' on the surface of the material was measured. When the thickness of the rear air layer was set to L_0, Z_2 was the impedance at the rear of the material, and Z_2' was similarly obtained. The thickness of the material is shown by b:

$$Z_c = \pm\sqrt{\frac{Z_1 Z_1'(Z_2 - Z_2') - Z_2 Z_2'(Z_1 - Z_1')}{(Z_2 - Z_2') - (Z_1 - Z_1')}}, \tag{4}$$

$$\gamma = \frac{1}{2b}\ln\left(\frac{Z_1 + Z_c}{Z_1 - Z_c}\frac{Z_2 - Z_c}{Z_2 + Z_c}\right). \tag{5}$$

The measured values of effective density $\rho(\omega)$ and bulk modulus $K(\omega)$ were derived from the characteristic impedance Z_c and the propagation constant γ. Eq. (6) shows the relationships among Z_c, $\rho(\omega)$ and $K(\omega)$, while Eq. (7) shows the relational expression of the complex wave velocity $c(\omega)$ and the propagation constant γ. Eqs. (8) and (9) can be derived from Eqs. (6) and (7), respectively,

$$Z_c = \rho(\omega)c(\omega) = [K(\omega)\rho(\omega)]^{1/2}, \tag{6}$$

$$\gamma = \mathrm{i}[\omega/c(\omega)], \tag{7}$$

$$\rho(\omega) = \frac{Z_c\gamma}{\mathrm{i}\omega}, \tag{8}$$

$$K(\omega) = Z_c^2/\rho(\omega). \tag{9}$$

The effective density of the Johnson–Allard model was replaced with that of the measurements and the propagation constant and characteristic impedance for an experiment model were calculated. The flow resistivity influences the imaginary part for the effective density, having a major influence on the propagation constant and characteristic impedance. Fig. 4 shows the results of sample 6; flow resistivity of the sample is 69,900 Pa s m^{-2}. The calculated and measured values were very close. As for the Johnson–Allard model, this result showed that both the real and imaginary parts of the effective density should be improved. Fig. 5 shows the results of sample 15; flow resistivity of the sample is 5700 Pa s m^{-2}. The calculated values were not close to the measured values, although improvements in the Johnson–Allard model were apparent. Fig. 5a shows the attenuation constant of sample 15. The attenuation constant was not especially suitable when based only on the combination of the measured values of the effective density with the bulk modulus of the Johnson–Allard model.

When the flow resistivity was 15,000 Pa s m^{-2} or more, excellent prediction accuracy was obtained by changing the effective density of the Johnson–Allard model to the measured values. However, it was necessary to improve both the effective density and the bulk modulus of the Johnson–Allard model when the flow resistivity was less than 15,000 Pa s m^{-2}. In particular, when the flow resistivity was less than 10,000 Pa s m^{-2}, improvement in the bulk modulus of the Johnson–Allard model was found to be important, and appeared clearly in Fig. 5.

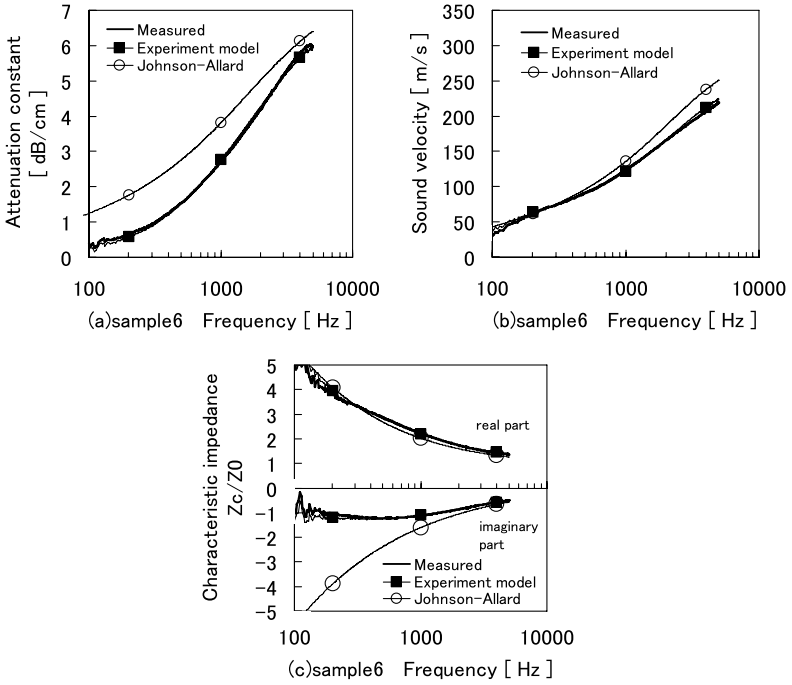

Fig. 4. Comparison among the measurements, the predicted values by the experiment model, and those of the Johnson–Allard model: (a) attenuation constant of sample 6; (b) sound velocity of sample 6; and (c) characteristic impedance of sample 6. Experiment model: the effective density used the measured value, and the bulk modulus used the values predicted by the Johnson–Allard model.

3. Theory and comparisons with data

Eq. (10) is the effective density of rigid-framed materials at an audible frequency, as proposed by Johnson et al. [3]:

$$\rho(\omega) = \rho_0 \alpha_\infty \left(1 + \frac{\sigma\phi}{\mathrm{i}\alpha_\infty \rho_0 \omega} G_J(\omega)\right), \tag{10}$$

with

$$G_J(\omega) = \left(1 + \frac{4\mathrm{i}\alpha_\infty^2 \eta \rho_0 \omega}{\sigma^2 \Lambda^2 \phi^2}\right)^{1/2}, \tag{11}$$

$$\wedge = s(8\eta\alpha_\infty/\sigma\phi)^{1/2}. \tag{12}$$

Eq. (13) is of the bulk modulus of rigid-framed materials, at an audible frequency, as proposed by Allard et al. [4]:

$$K(\omega) = \gamma P_0 \Big/ \left[\gamma - (\gamma - 1)\left[1 + \frac{\sigma'\phi}{\mathrm{i}\alpha_\infty \rho_0 Pr\omega} G'_J(Pr\omega)\right]^{-1}\right], \tag{13}$$

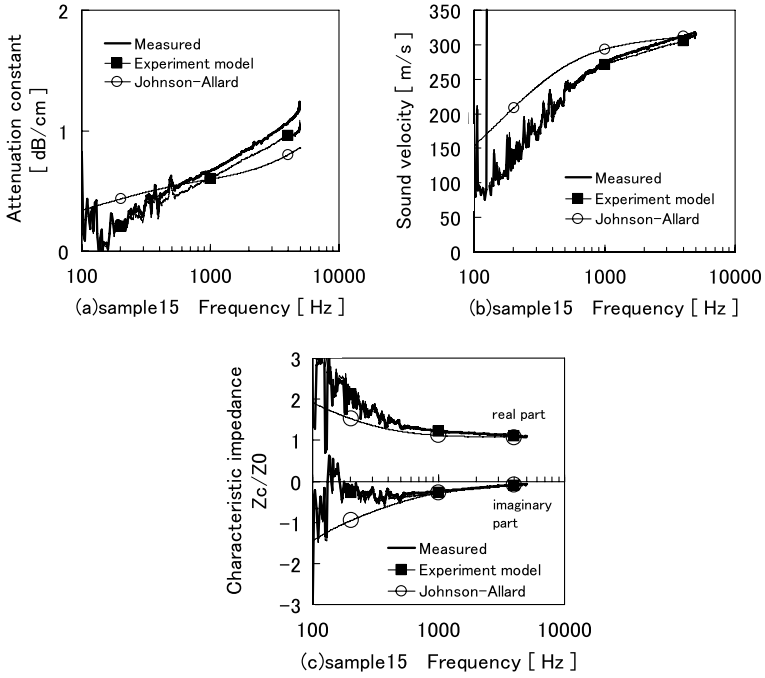

Fig. 5. Comparison among the measurements, the predicted values by the experiment model, and those of Johnson–Allard model: (a) attenuation constant of sample 15; (b) sound velocity of sample 15; and (c) characteristic impedance of sample 15. Experiment model: the effective density used the measured values, and the bulk modulus used the values predicted by the Johnson–Allard model.

with

$$G'_J(Pr\omega) = \left(1 + \frac{4i\alpha_\infty^2 \eta\rho_0 Pr\omega}{\sigma'^2 \Lambda'^2 \phi^2}\right)^{1/2}, \tag{14}$$

$$\Lambda' = s'(8\eta\alpha_\infty/\sigma\phi)^{1/2}, \tag{15}$$

$$s' = (\sigma/\sigma')^{1/2}, \tag{16}$$

where ρ_0 is the density of a gas, σ is the flow resistivity, ω is the angular frequency, $i = \sqrt{-1}$, η is the viscosity of a gas, P_0 is the atmospheric pressure, and s and s' are the cross-sectional shape factors of the pore. Eqs. (10)–(16) are the Johnson–Allard model. Eqs. (13) and (14) can be rewritten to the following equation [6].

$$K(\omega) = \gamma P_0 \Bigg/ \left[\gamma - (\gamma - 1)\left[1 + \frac{8\eta}{i\Lambda'^2 \rho_0 Pr\omega} G'_J(Pr\omega)\right]^{-1}\right], \tag{17}$$

with

$$G'_J(Pr\omega) = \left(1 + \frac{i\rho_0 \Lambda'^2 Pr\omega}{16\eta}\right)^{1/2}. \tag{18}$$

Eq. (10) was analysed and Eq. (11) was transformed as follows:

$$G_J(\omega) = (1 + \mathrm{i}d)^{1/2} = e + \mathrm{i}f, \tag{19}$$

with

$$d = \frac{4\alpha_\infty^2 \eta \rho_0 \omega}{\sigma^2 \Lambda^2 \phi^2}, \tag{20}$$

where e and f are variables.

When both sides of Eq. (19) were squared, Eq. (21) was obtained:

$$1 + \mathrm{i}d = (e + \mathrm{i}f)^2. \tag{21}$$

By solving Eq. (21), Eqs. (22) and (23) were obtained:

$$e = \sqrt{\frac{1 + \sqrt{1 + d^2}}{2}}, \tag{22}$$

$$f = \frac{d}{2e}. \tag{23}$$

By using Eq. (20) for Eq. (22), Eq. (24) was obtained:

$$e = \left[\frac{1}{2}\left(1 + \left[1 + \left(\frac{4\alpha_\infty^2 \eta \rho_0 \omega}{\sigma^2 \Lambda^2 \phi^2}\right)^2\right]^{1/2}\right)\right]^{1/2}. \tag{24}$$

By using Eq. (20) for Eq. (23), Eq. (25) was obtained:

$$f = \frac{1}{2e}\frac{4\alpha_\infty^2 \eta \rho_0 \omega}{\sigma^2 \Lambda^2 \phi^2}. \tag{25}$$

By using Eq. (25) for Eq. (19), Eq. (26) was obtained:

$$G_J(\omega) = e + \mathrm{i}f = e + \mathrm{i}\frac{1}{2e}\frac{4\alpha_\infty^2 \eta \rho_0 \omega}{\sigma^2 \Lambda^2 \phi^2}. \tag{26}$$

By using Eq. (26) for Eq. (10), Eq. (27) was thus obtained:

$$\rho(\omega) = \rho_0\left(\alpha_\infty + \frac{1}{e}\frac{2\alpha_\infty^2 \eta}{\sigma\phi\Lambda^2} - \mathrm{i}e\frac{\sigma\phi}{\omega\rho_0}\right). \tag{27}$$

Therefore, the high frequency limit of Eq. (10) is Eq. (28). The low frequency limit of Eq. (10) is Eq. (29):

$$\lim_{\omega\to\infty}\rho(\omega) = \rho_0\alpha_\infty, \tag{28}$$

$$\lim_{\omega\to\infty}\rho(\omega) = \rho_0\left(\alpha_\infty + \frac{2\alpha_\infty^2 \eta}{\sigma\phi\Lambda^2} - \mathrm{i}\frac{\sigma\phi}{\omega\rho_0}\right). \tag{29}$$

For rigid-framed fibrous materials, the necessary conditions required to achieve predictions of effective density with good precision are the asymptotic behaviour at low frequencies of both the real and imaginary parts of Eq. (10). According to the Johnson–Allard model, the imaginary part is predicted to have asymptotic behaviour at low frequencies; however, it also predicts that the real part is constant at low frequencies, showing considerable difference from the measurements.

At high frequencies, the equation for the effective density is given by Eq. (30), as proposed by Johnson et al. [3]. Further, at high frequencies the equation of the bulk modulus is given by Eq. (31), as proposed by Allard et al. [4]. The complex wave number [9] is given by Eq. (32), which can be derived from Eqs. (30) and (31):

$$\rho(\omega)_{\text{high}} = \rho_0\alpha_\infty[1 + (1 - \mathrm{i})(\delta/\wedge)], \tag{30}$$

$$K(\omega)_{\text{high}} = \gamma P_0/[1 + (\gamma - 1)(1 - \mathrm{i})(\delta/\sqrt{Pr}\wedge')], \tag{31}$$

$$k_{\text{high}} = \frac{\omega}{c_0}\sqrt{\alpha_\infty}\left[1 + (1 - \mathrm{i})\frac{\delta}{2}\left(\frac{1}{\wedge} + \frac{\gamma - 1}{\sqrt{Pr}\wedge'}\right)\right], \tag{32}$$

with

$$\delta = (2\eta/\omega\rho_0)^{1/2}. \tag{33}$$

With this in mind, we improved Eq. (10) proposed by Johnson by using Eq. (30). When Eq. (30) is transformed into the shape of Eq. (10), Eq. (34) is obtained:

$$\rho(\omega)_{\text{high}} = \rho_0\alpha_\infty\left(1 + \frac{\sigma\phi}{\mathrm{i}\alpha_\infty\rho_0\omega}G_{J(H)}(\omega)\right), \tag{34}$$

with

$$G_{J(H)}(\omega) = \sqrt{2\eta\rho_0\omega}\frac{\alpha_\infty(1 + \mathrm{i})}{\sigma\phi\wedge}. \tag{35}$$

We improved Eq. (11) by using Eq. (35). Johnson proposed Eq. (10) as the simplest possible model [3] considering the low and high frequency limits. We also considered the high frequency limit $\rho_0\alpha_\infty$ along with asymptotic behaviour at the low frequency limit. We propose Eq. (36) as a new model. In addition, the bulk modulus has been similarly improved, and we propose Eq. (39) as a new model. Correction factors N_1 and N_2 that were functions of flow resistivity were created. The approximation curves were drawn on a graph using a MATLAB curve fitting toolbox, as shown in Fig. 6. The Johnson–Allard formula for effective density and bulk modulus were modified using the correction factors:

$$\rho(\omega) = \rho_0\alpha_\infty\left(1 + \frac{\sigma\phi}{\mathrm{i}\alpha_\infty\rho_0\omega}G_N(\omega)\right), \tag{36}$$

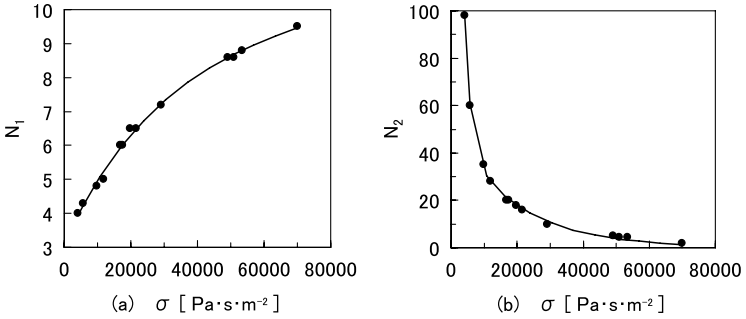

Fig. 6. Approximation curve obtained from the seven glass wool samples and the six polyester fibre samples: (a) N_1 and (b) N_2.

with

$$G_N(\omega) = \left(\sqrt{2\eta\rho_0\omega}\frac{\alpha_\infty(1+\mathrm{i})\sqrt{N_1}}{\sigma\phi\wedge}\right)^{1/2}, \tag{37}$$

$$N_1 = 8.622\exp(1.969\times10^{-6}\sigma) - 5.54\exp(-3.682\times10^{-5}\sigma), \tag{38}$$

where N_1 is an empirical function of flow resistivity obtained by fitting data.

$$K(\omega) = \gamma P_0 \Bigg/ \left[\gamma - (\gamma-1)\left[1 + \frac{8\eta}{\mathrm{i}\wedge'^2\rho_0 Pr\omega}G'_N(Pr\omega)\right]^{-1}\right], \tag{39}$$

with

$$G'_N(Pr\omega) = \left(\sqrt{2\eta\rho_0 Pr\omega}\frac{\alpha_\infty(1+\mathrm{i})\sqrt{N_2}}{\sigma'\phi\wedge'}\right)^{1/2} = \left(\sqrt{2\eta\rho_0 Pr\omega}\frac{\wedge'(1+\mathrm{i})\sqrt{N_2}}{8\eta}\right)^{1/2}, \tag{40}$$

$$N_2 = 560.3\exp(-5.565\times10^{-4}\sigma) + 50.02\exp(-5.127\times10^{-5}\sigma), \tag{41}$$

where N_2 is an empirical function of flow resistivity obtained by fitting data.

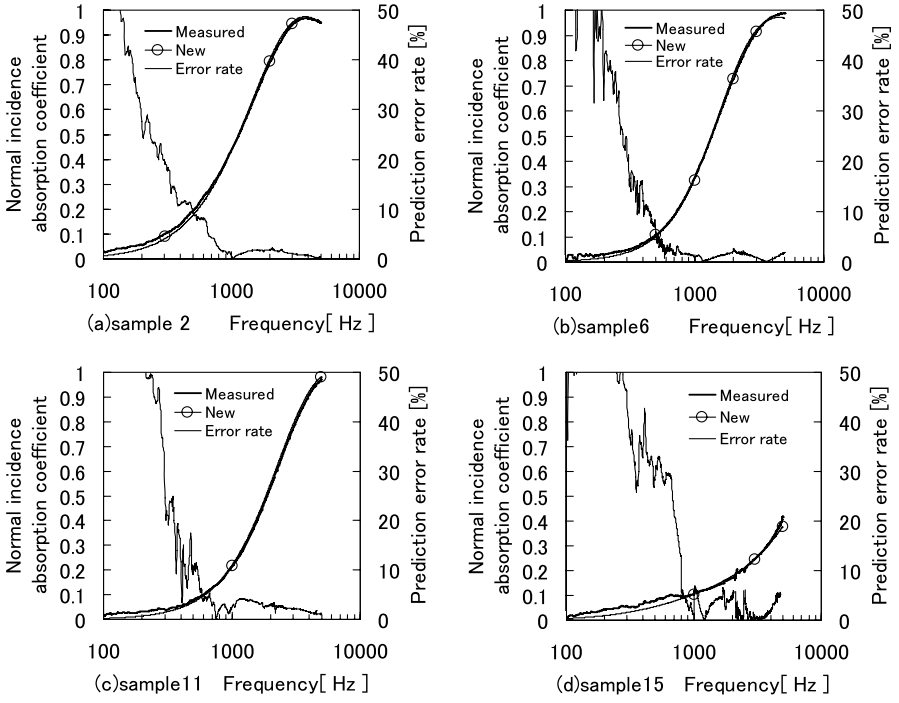

Fig. 7. Comparison of normal incidence absorption coefficients for hard-backed material samples, between the values as measured and those predicted, by the new model as a function of frequency: (a) sample 2 of glass wool; (b) sample 6 of glass wool; (c) sample 11 of polyester fibre; and (d) sample 15 of polyester fibre.

4. Results and discussion

The prediction error of the normal incidence absorption coefficient for hard-backed material samples of the new model was derived in the frequency range between 100 Hz and 5 kHz. The comparative results are shown in Fig. 7. The mean value of the prediction error of sample 2 shown in Fig. 7a was 3.2%; that of sample 6 shown in Fig. 7b was 3.6%; that of sample 11 shown in Fig. 7c was 5.1%; and that of sample 15 shown in Fig. 7d was 7.6%. The range of 5% or less in the prediction error of sample 2 shown in Fig. 7a was at

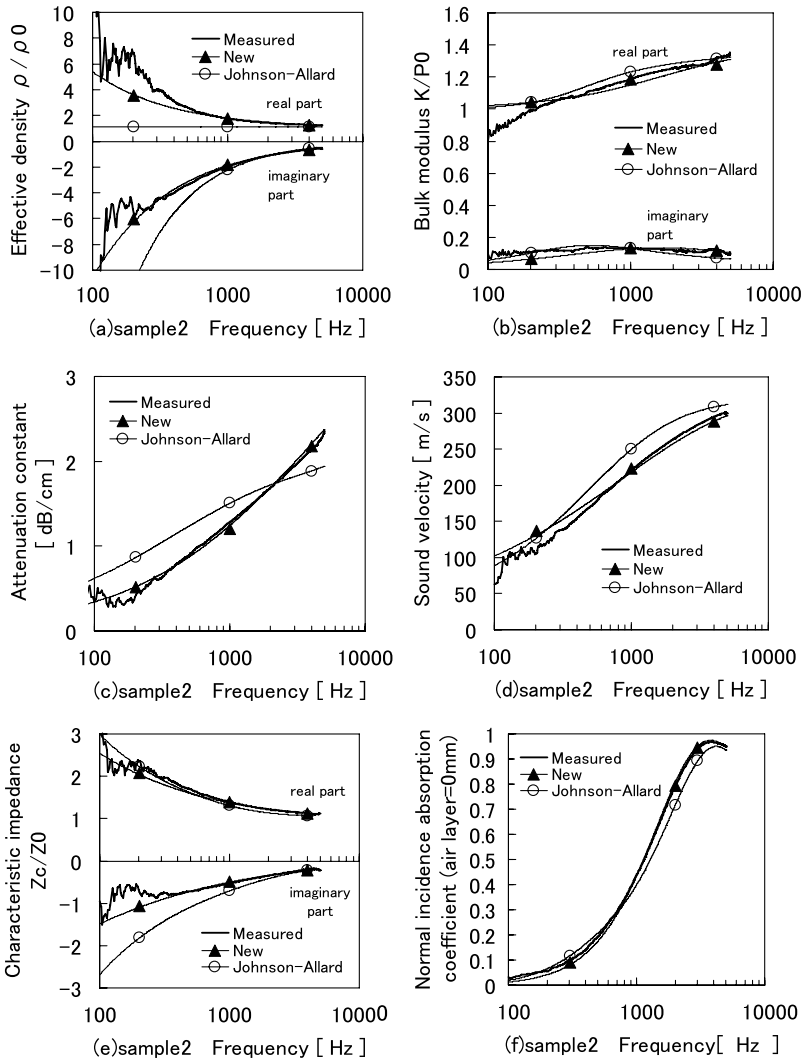

Fig. 8. Comparison among the measured values, the values predicted by the new model and those by the Johnson–Allard model. $N_1 = 5.9$ and $N_2 = 21.2$. The material is glass wool. Bulk density was 31.8 kg m^{-3}. Flow resistivity was 16,800 Pa s m^{-2}. Thickness was 25.0 mm: (a) effective density; (b) bulk modulus; (c) attenuation constant; (d) sound velocity; (e) characteristic impedance; and (f) absorption coefficient.

frequencies more than 660 Hz; that of sample 6 shown in Fig. 7b was at frequencies more than 500 Hz; that of sample 11 shown in Fig. 7c was at frequencies more than 584 Hz; and that of sample 15 shown in Fig. 7d was at frequencies more than 800 Hz.

Figs. 8–11 show comparison results among the measured values, the predicted values of our new model, and the predicted values of the Johnson–Allard model. The temperature was 25 °C during the experiment; based on this, the acoustic impedance Z_0 of air in four figures was 411 kg m^{-2} s^{-1}. Each figure shows comparison results of the effective density,

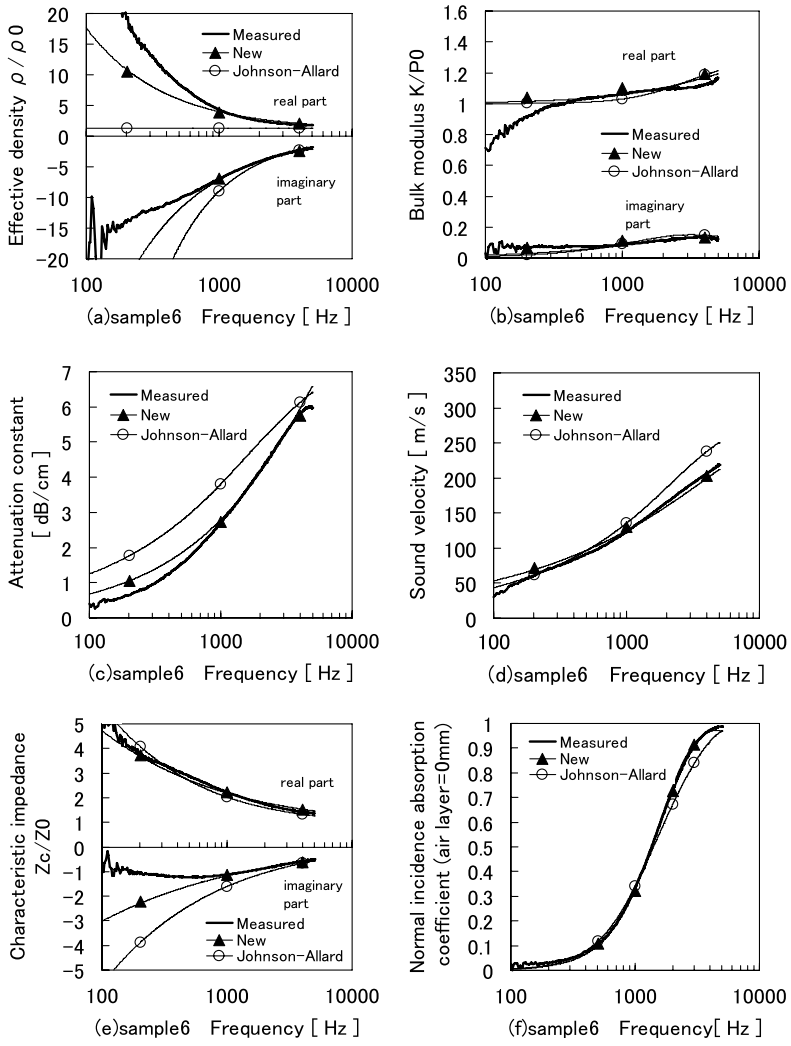

Fig. 9. Comparison among the measured values, the values predicted by the new model and those obtained by the Johnson–Allard model. $N_1 = 9.5$ and $N_2 = 1.4$. The material is glass wool. Bulk density was 101.2 kg m^{-3}. Flow resistivity was 69,900 Pa s m^{-2}. Thickness was 14.0 mm: (a) effective density; (b) bulk modulus; (c) attenuation constant; (d) sound velocity; (e) characteristic impedance; and (f) absorption coefficient.

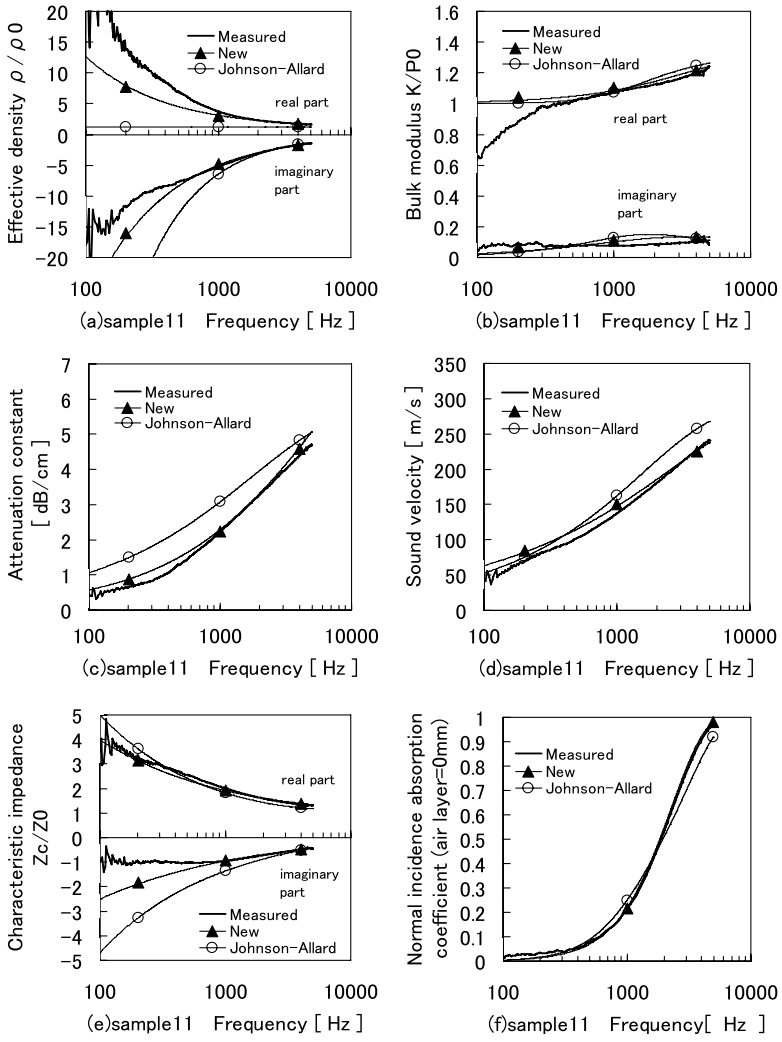

Fig. 10. Comparison among the measured values, the values predicted by the new model and those obtained by the Johnson–Allard model. $N_1 = 8.7$ and $N_2 = 3.7$. The material is polyester fibre. Bulk density was 72.9 kg m^{-3}. Flow resistivity was 51,000 Pa s m^{-2}. Thickness was 12.5 mm: (a) effective density; (b) bulk modulus; (c) attenuation constant; (d) sound velocity; (e) characteristic impedance; and (f) absorption coefficient.

bulk modulus, attenuation constant, phase velocity, characteristic impedance and normal incidence absorption coefficient for hard-backed material samples.

Based on the results of the normal incidence absorption coefficient, as shown in figure f, the prediction accuracy of our new model was superior to that of the Johnson–Allard model. The real part of the effective density of the Johnson–Allard model, as shown in figure a, remains constant in all four graphs. The measured values of the real part of the effective density show asymptotic behaviour at low frequencies. The attenuation constant of the Johnson–Allard model, as shown in figure c, differs greatly from the measured value in all of the four graphs. Likewise, for the Johnson–Allard model the phase velocity

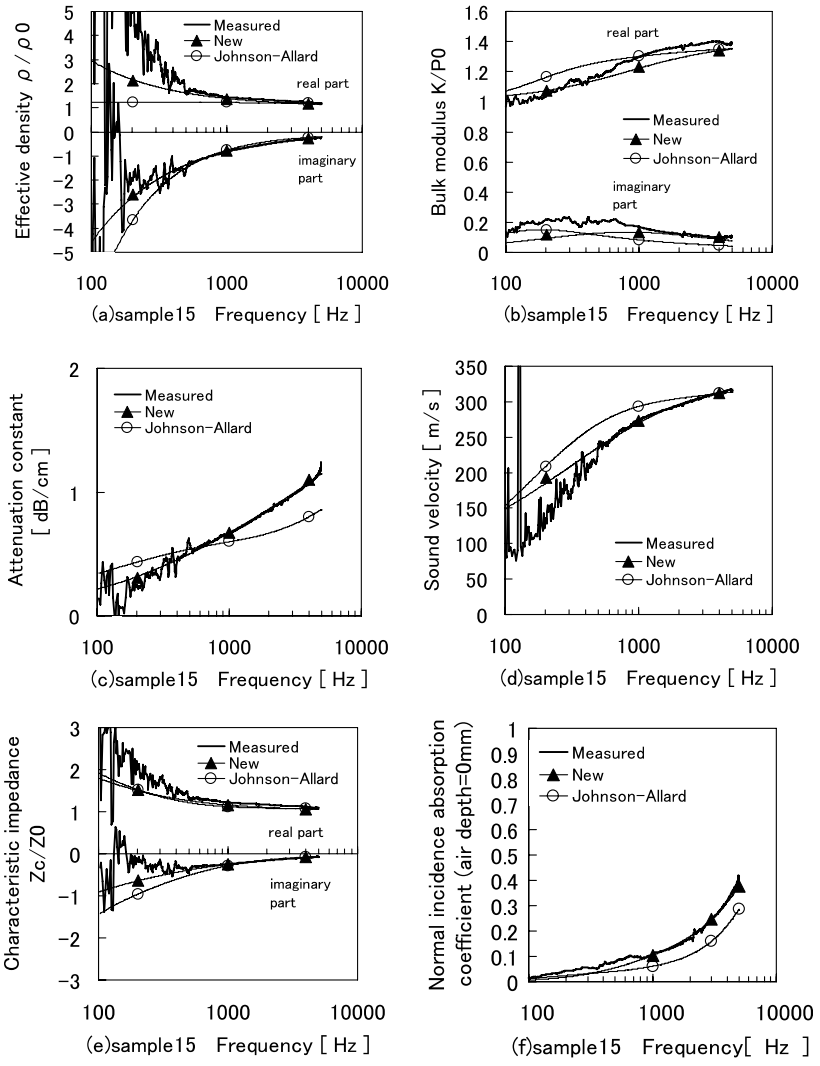

Fig. 11. Comparison among the measured values, the values predicted by the new model and those obtained by the Johnson–Allard model. $N_1 = 4.2$ and $N_2 = 61$. The material is polyester fibre. Bulk density was 64.4 kg m^{-3}. Flow resistivity was 5700 Pa s m^{-2}. Thickness was 11.0 mm: (a) effective density; (b) bulk modulus; (c) attenuation constant; (d) sound velocity; (e) characteristic impedance; and (f) absorption coefficient.

and the imaginary part of the characteristic impedance differ from the measured values. The prediction of the normal incidence absorption coefficient, namely that our accuracy is better than the Johnson–Allard model, was achieved, which indeed was the purpose of this study.

When the comparative results of the normal incidence absorption coefficient that assumes a rear air layer of 20 mm, as shown in Fig. 12, is seen, the difference between the value predicted by the Johnson–Allard model and the measured value is clearly understood. In Fig. 12 the prediction error of our new model is less than 5% in the frequency

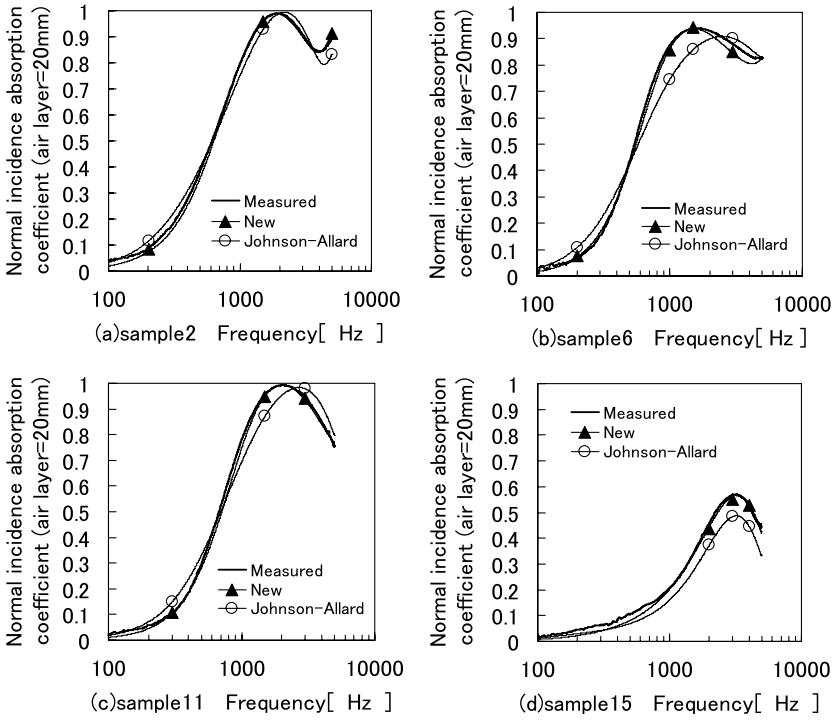

Fig. 12. Comparison among the measured values, the values predicted by the new model and those predicted by the Johnson–Allard model. Normal incidence absorption coefficients that take the rear air layer as 20 mm are shown: (a) glass wool of sample 2; (b) glass wool of sample 6; (c) polyester fibre of sample 11; (d) polyester fibre of sample 15.

range between 800 Hz and 5 kHz. The prediction error of the Johnson–Allard model in the frequency range of 4.4 kHz or more exceeds 7% in Fig. 12a, and the error in the frequency range between 800 Hz and 1 kHz exceeds 15% in Fig. 12b. The prediction error in the frequency range between 860 Hz and 1.4 kHz by the Johnson–Allard model exceeds 10% in Fig. 12c. Additionally, the prediction error in the frequency range between 800 Hz and 5 kHz by the Johnson–Allard model shows a value from 15% to 20% in Fig. 12d.

5. Concluding remarks

The Johnson–Allard model for rigid-framed fibrous materials uses porosity, flow resistivity, tortuosity and two characteristic lengths. Using measured values of these parameters only predictions of normal absorption coefficient were found to be in tolerable agreement with measurements whereas predictions of normal surface impedance have been found to be relatively poor. Therefore, effective density, bulk modulus, propagation constant and characteristic impedance were examined using seven glass wool samples and six polyester fibre samples. It was difficult to obtain good precision in the predictions for materials having low flow resistivity. In this paper, a new model has been proposed. The prediction error using our new model was 5% or less in the frequency range between 800 Hz and 5 kHz. The proposed new model has been shown to be more accurate than Johnson–Allard also for prediction of normal incidence absorption coefficient.

Acknowledgement

The authors thank Mr. Nobuhiro Ohba.

References

[1] Delany ME, Bazley EN. Acoustical properties of fibrous absorbent materials. Appl Acoust 1970;3:105–16.
[2] Miki Y. Acoustical properties of porous materials – generalizations of empirical models. J Acoust Soc Jpn 1990;E11:25–8.
[3] Johnson DL, Koplik J, Dashen R. Theory of dynamic permeability and tortuosity in fluid-saturated porous media. J Fluid Mech 1987;176:379–402.
[4] Champoux Y, Allard JF. Dynamic tortuosity and bulk modulus in air-saturated porous media. J Appl Phys 1991;70:1975–9.
[5] Allard JF, Champoux Y. New empirical equations for sound propagation in rigid frame fibrous materials. J Acoust Soc Am 1992;91:3346–53.
[6] Lafrage Denis, Allard JF, Brouard Bruno. Characteristic dimensions and prediction at high frequencies of the surface impedance of porous layers. J Acoust Soc Am 1993;93:2474–8.
[7] Henry M, Lemarinier Pavel, Allard JF, Bonardet JL, Gedeon A. Evaluation of the characteristic dimensions of porous sound-absorbing materials. J Appl Phys 1995;77:17–20.
[8] ISO 9053:1991. Acoustics – materials for acoustical applications – determination of airflow resistance.
[9] Leclaire Ph, Keiders L, Lauriks W. Determination of the viscous and thermal characteristic lengths of plastic foams by ultrasonic measurements in helium and air. J Appl Phys 1996;80:2009–12.
[10] Allard JF, Castagnede B, Henry M, Laurinks W. Evaluation of tortuosity in acoustic porous materials saturated by air. Rev. Sci. Instrum. 1994;65:754–5.
[11] ISO 10534-2:1998. Acoustics – determination of sound absorption coefficient and impedance in impedance tubes – Part2: transfer-function method.
[12] Utsuno H, Tanaka T, Fujikawa T, Seybert AF. Transfer function method for measuring characteristic impedance and propagation constant of porous materials. J Acoust Soc Am 1989;86:637–43.